Monthly Notices
of the
ROYAL ASTRONOMICAL SOCIETY

MNRAS **494,** 1448–1462 (2020)
Advance Access publication 2020 March 28

doi:10.1093/mnras/staa833

Inferred time-scales for common envelope ejection using wide astrometric companions

Andrei P. Igoshev [1,2]★ Hagai B. Perets [1] and Erez Michaely [3]

[1] *Physics Department, Technion – Israel Institute of Technology, Haifa 3200002, Israel*
[2] *Department of Applied Mathematics, University of Leeds, Leeds LS2 9JT, UK*
[3] *Astronomy Department, University of Maryland, College Park, MD 20742, USA*

Accepted 2020 March 21. Received 2020 February 24; in original form 2019 July 23

ABSTRACT

Evolution of close binaries often proceeds through the common envelope stage. The physics of the envelope ejection (CEE) is not yet understood, and several mechanisms were suggested to be involved. These could give rise to different time-scales for the CEE mass-loss. In order to probe the CEE-time-scales we study wide companions to post-CE binaries. Faster mass-loss time-scales give rise to higher disruption rates of wide binaries and result in larger average separations. We make use of data from *Gaia* DR2 to search for ultrawide companions (projected separations 10^3–2×10^5 au and $M_2 > 0.4\,\mathrm{M}_\odot$) to several types of post-CEE systems, including sdBs, white dwarf post-common binaries, and cataclysmic variables. We find a (wide-orbit) multiplicity fraction of 1.4 ± 0.2 per cent for sdBs to be compared with a multiplicity fraction of 5.0 ± 0.2 per cent for late-B/A/F stars which are possible sdB progenitors. The distribution of projected separations of ultrawide pairs to main sequence stars and sdBs differs significantly and is compatible with prompt mass-loss (upper limit on common envelope ejection time-scales of 10^2 yr). The smaller statistics of ultrawide companions to cataclysmic variables and post-CEE binaries provide weaker constraints. Nevertheless, the survival rate of ultrawide pairs to the cataclysmic variables suggest much longer, $\sim 10^4$ yr time-scales for the CEE in these systems, possibly suggesting non-dynamical CEE in this regime.

Key words: binaries: general – stars: low-mass – stars: mass-loss – stars: statistics.

1 INTRODUCTION

The common envelope (CE) stage is an important stage in binary evolution, occurring in close binaries, typically when the primary evolves off the main sequence and expands. It gives rise to short period binaries, and drives the mergers of stars either directly or through the later evolution of post-CE compact remnant binaries that merge through gravitational-wave emission. For a CE to ensue, the envelope needs to overflow the Roche lobe as to initiate a mass transfer to the companion. If and when the mass transfer is unstable, the primary's envelope engulfs the binary companion as to give rise to a CE. The following dynamical evolution is then driven by the gas drag force and gravity (Paczynski 1976) leading to the inspiral of the binary. The inspiral stage results in the binary merger or in the formation of a tight post-common envelope (pCE) binary (for a most recent review see Ivanova et al. 2013).

Purely hydrodynamical simulations do not give rise to the full ejection of the CE, in contrast with the observations of naked post-CE binaries (Ivanova et al. 2013). Such difficulties lead to the introduction of possible additional processes that may play a role in the CEE. These include the effects of recombination, dust-driven winds, or jets (see Glanz & Perets 2018 for a brief overview).

Here we consider several types of systems which likely went through a CE stage. In the case when the primary is low-mass star, the naked helium core is seen for a short time as subdwarf B stars (sdBs) before it turns into a white dwarf (WD), and therefore sdB stars are likely result of a post-CE evolution, a remnant post-CE WD could undergo a mass transfer from a close secondary star, in which case it is likely to manifest itself as a cataclysmic variable (CV, for review see Ritter 2010). Finally, a non-accreting short-period WD binary is another possible post-CE product.

The mass ejection during the CEE is typically thought to occur at relatively short (dynamical) time-scales comparable to the inspiral time of the secondary or somewhat longer. If only a part of the envelope mass is ejected at the dynamical time-scale, the CE could be initiated multiple times and, therefore, the mass-loss time-scale becomes longer. However, the time-scale of CE, the minimum companion mass, and the fraction of pre-CE to post-CE binary separations are not yet constrained observationally. Recently, Michaely & Perets (2019) tried to probe the time-scale using two pCE binaries with additional wide astrometric components,

★ E-mail: ignotur@gmail.com

i.e. using wide triple systems. We aim at extending this analysis and search for common proper motion and parallax pairs to pCE binaries, sdBs, and CVs using a large sample based on the *Gaia* second data release (Gaia Collaboration 2016, 2018).

When the inner binary in a hierarchical triple enters the CE stage, the mass ejection strongly affects orbit of the distant third companion. We expect that the distribution of projected separations for ultrawide components and fraction of survived ultrawide components will therefore differ between the case of binaries which did not go through a CEE and ones which did lose mass through the CEE process.

Approximately 10 per cent of solar mass stars are born as hierarchical triples (Moe & Di Stefano 2017). This fraction reaches up to 20 per cent for stars extending to four solar masses. Triples are also known among systems which went through the CE evolution such as Wolf 1130 (Mace et al. 2013) and GD 319 (Farihi, Becklin & Zuckerman 2005). These third components have orbital separations of $\approx 3.2 \times 10^3$ au in the case of Wolf 1130 and $\approx 5.5 \times 10^4$ au in the case of GD 319. Triples are also found among the sdB stars; for example, PG 1253+284 is seen as resolved pair with a separation of 0.24 arcsec and additionally shows radial velocity variations (Heber et al. 2002). Another possible case is SDSS J095101.28+034757.0 (Kupfer et al. 2015) which shows an excess of IR radiation.

In the following we explore wide companions statistics using large samples. Our analysis follows similar ideas used in the work of El-Badry & Rix (2018) who studied the projected separation of ultrawide companions to WDs in order to infer natal kick magnitudes of WDs. Such analysis can provide the first statistical constraints on the CEE mass-loss time-scales based on large samples.

The paper is structured as follows: in Section 2 we summarize the formation scenarios for systems which experience CEE. In Section 3 we describe our data set and in Section 4 we describe our method to search for ultrawide binaries using the second *Gaia* data release. In Section 5 we describe the results of our search for ultrawide components. In Section 6 we perform a simple simulation for orbital evolution of triple systems with a significant mass-loss from the inner binary and we conclude with results and discussions in Section 7.

2 FORMATION PATHS OF POST COMMON ENVELOPE BINARIES

In this Section we briefly describe scenarios suggested to explain the formation of post-common envelope binaries with a white dwarf and sdB stars.

2.1 Formation of post-common envelope binaries with a white-dwarf component

Low-mass white dwarfs with mass less than $\approx 0.5\,M_\odot$ should form through isolated stellar evolution only on time-scales which greatly exceed the Hubble time-scale. Nevertheless, low-mass WDs are not rare among main sequence – white dwarf binaries (MSWD) and contain up to a third of the observed population (see Rebassa-Mansergas et al. 2016). The MSWD sample is not complete and the actual fraction might differ due to various selection effects. The most natural explanation for their formation is through a CEE in binary systems when the more massive primary star losses its extended hydrogen envelope at the subgiant stage due to interaction of the envelope with the secondary main sequence star, leaving behind the He core which later becomes a low-mass, typically He-rich WD (e.g. Zenati, Toonen & Perets (2019) and references therein). Such binaries are seen as composite spectra binaries with large, periodic radial velocity variations observed through their optical spectra or as eclipsing binaries with reflection effects seen in the light-curve, e.g. HW Vir type systems (Heber 2016).

2.2 Formation of sdB stars

sdB stars are low-mass stars ($M \approx 0.5\,M_\odot$; Heber 1986, 2016) located to the left of the main sequence at the Hertzsprung Russell diagram around absolute magnitude of ≈5. Most of these stars are considered to be helium-core burning stars with thin hydrogen envelopes which contain $<0.02\,M_\odot$ (Saffer et al. 1994). Such sdB stars experience a significant mass-loss and many of them are found in close binaries with orbital periods of less than 10 d, which suggests a formation through a CE stage.

Following classical stellar evolution theory, an isolated red giant is not expected to lose its envelope and turn into a helium burning core. Therefore, the theories for the sdB formation include either non-standard stellar evolution (helium mixing, hot-flash) or the presence of the secondary companion which serves to strip the sdB stellar progenitors. When an sdB star is observed to be part of a close binary, the secondary star had to play an important role in the sdB formation. Indeed, recent radial velocity measurements (Napiwotzki et al. 2004; Copperwheat et al. 2011) discovered a large binarity fraction among sdB stars with up 50 per cent or higher. In most cases the binary companions cannot be directly detected, consistent with most of them being WDs or M dwarfs.

Several binary evolution scenarios were suggested for the origin of sdB stars (Han et al. 2002). These include CE evolution (Paczynski 1976), leading to the formation of very short-period binaries with orbital periods of less than 10 d; Roche lobe overflow leading to the formation of wider binaries and mergers of two helium WDs (Webbink 1984), leading to the formation of single/isolated sdB stars. It is thought that CEE plays a key role in most cases and that up to 2/3 of known sdBs (Han et al. 2002) are formed through this process. The expected mass of sdB progenitors (Han et al. 2003) range between $0.9\,M_\odot$ (the lightest star which could form a red giant on time-scales smaller than the Hubble time) to $\approx 3\,M_\odot$. sdBs formed from a more massive progenitors are expected to be rare because of the initial mass function, shorter lifetime of massive He stars, and other selection effects. Moreover systems with more massive progenitors are classified as sdO and Wolf-Rayet stars (Götberg et al. 2019).

2.3 Cataclysmic variables

A typical cataclysmic variable contains a CO WD component with a mass of $\approx 1\,M_\odot$ and a secondary with a mass of $\approx 1\,M_\odot$ (Ritter 2010). The CO WD is, therefore, thought to originate from a primary in the mass range $2.2 - 8\,M_\odot$ because these WDs are formed following the complete loss of the hydrogen-rich envelope at the AGB stage before the carbon burning has started (Ritter 2010). A CV might alternatively contain an ONe WD in which case it might have formed from even more massive stars.

The CE is initiated when the primary expands during its post-MS evolution. After the end of the CE, the semimajor axis of the binary shrinks following the loss of angular momentum through magnetic braking and/or gravitational wave emission. At some point the secondary fills its Roche lobe and a second mass transfer epoch is initiated. This second mass transfer is usually stable and the binary is seen as CV at this stage.

3 DATA

In the following we describe the data collected for the various type of post-CE objects discussed above.

3.1 Main sequence – white dwarf binaries

We use the catalogue of MSWD binaries compiled by Rebassa-Mansergas et al. (2007), (2012), (2013), (2016).[1] This catalogue includes 3287 MSWD binaries identified in the Sloan Digital Sky Survey (York et al. 2000). Only ≈25 per cent of MSWD binaries are classified as post-CE systems. This small fraction is a consequence of the technique applied: Rebassa-Mansergas et al. (2007) considered that an MSWD is a possible post-CE system only if it was observed during multiple epochs and it showed radial velocity variations. Meanwhile, among ≈3000 MSWD systems only ≈600 were observed during multiple epochs. In order to get the parallaxes and proper motions for these stars we match these data with the second *Gaia* data release (Gaia Collaboration 2016, 2018). All details of the cross-match are summarized in Appendix A.

3.2 Hot subdwarf systems

We use the catalogue of sdBs by Geier et al. (2019). This catalogue contains 39 800 candidates selected in *Gaia* DR2 and includes some possible contamination at the level of 10 per cent. Only 9826 objects from this catalogue satisfy our quality cuts (where we require the relative errors in the parallax and in the proper motion measurements to be below 0.25). The measured parallaxes range from 0.1 mas up to 56 mas. In order to be sensitive to ultrawide binaries we select only systems with measured parallaxes larger than 0.66 mas. Also we exclude two systems: HD110698 and BD+164120B for which we had troubles accessing the *Gaia* data base. After these additional cuts we end up with 4709 systems.

We also tried to consider the recent catalogue by Kepler et al. (2019). Unfortunately, we manage to identify only 259 sdBs stars from this catalogue in the *Gaia* data base using SDSS i,g colours with the conversion by Jordi et al. (2010) within 3 arcsec from their catalogue positions. From this list of 259 stars only 69 have well measured parallax and proper motions which are suitable for our ultrawide binary search, but we found no ultrawide binary counterparts for any of them.

3.3 Cataclysmic variables

As a source for positions of cataclysmic variables we used the catalogue of Ritter & Kolb (2003) v.7.20[2] which contains 1429 objects. Because CVs are very variable in the optical band, we used only the coordinate information in our identification and did not perform magnitude or colour analysis. We searched for *Gaia* counterparts within 1.8 arcsec of the given catalogue positions and managed to identify 562 objects with good astrometric measurements of the parallax and the proper motion.

We also notice that some of sdB objects listed in catalogue by Geier et al. (2019) are in fact CVs and we exclude them from our analysis of sdBs.

[1] https://www.sdss-wdms.org
[2] http://www.mpa-garching.mpg.de/RKcat/

3.4 Comparison samples

Hierarchical triple systems with central pCE or MSWD wide binary originate from hierarchical main sequence systems. Therefore, we want to identify wide binaries to main sequence stars and compare their occurrence rates with wide binaries to pCE systems. We select three samples: (A) direct comparison to sdBs, (B) a sample of only close-by objects (parallax $\varpi > 5$ mas), and (C) more massive stars to be compared with CVs (which likely originate from more massive stars). The ADQL requests are summarized in Appendix A, B and C.

Comparison sample A contains 10 000 main sequence stars selected by the stellar radius and temperatures determined by the classification algorithm Apsis (Bailer-Jones et al. 2013; Andrae et al. 2018). We chose stars more massive than the Sun with masses 2–3 $M_\odot$ and with relative errors in parallax and proper motion measurements of less than 0.2. We also restrict the measured parallax to be in the range 0.67–10 mas as to select this sample in exactly the way we have selected the sdBs.

Comparison sample B contains 2452 stars with parallax $\varpi > 5$ and a relative error in parallax of less than 0.05. These stars are selected based on their colour and absolute magnitude which are not corrected for extinction. We could not use the results of the Apsis algorithm for this sample because only a small number of stars were successfully classified using it. This sample is selected in such a way as to resolve ultrawide binaries with separations of 10^2–10^3 au. These binaries are the type of possible progenitors for sdBs with tertiary ultrawide components at projected separations of few $\times 10^2$–10^4 au.

Comparison sample C contains 3399 stars. These are more massive stars (a minimal mass of 3.5 $M_\odot$, with a mean mass of $\approx 6\,M_\odot$, and a maximum mass of 9 $M_\odot$). Given the stellar initial mass function such stellar population is inherently less frequent and we therefore extended our selection up to parallax $\varpi > 2$ mas in order to be able to identify sufficient number of appropriate stars and be able to resolve pairs with projected separations of $\sim 10^2$ au. In order to select stars for this sample, we require the relative error in the parallax and the proper motion to be less than 0.1. The sample is used to simulate the survival fractions of CVs (which typically originate from these more massive stars) with ultrawide companions.

4 METHOD

We identify common proper motion and parallax pairs to MSWD, sdBs, and CVs stars following the method described in El-Badry & Rix (2018) and in our recent work (Igoshev & Perets 2019). We assume that two stars are likely to be gravitationally bound if they are located close at the sky, have similar parallaxes, and move in similar directions. Practically, we check if following criteria are satisfied: (1) their parallaxes differ by less than twice the error in the parallax difference; (2) the proper motion difference is less than twice the error in the proper motion difference plus the contribution due to the orbital motion; (3) the error in the parallax difference is below 0.6 mas; (4) the error in the proper motion difference is below two times the possible difference due to the orbital motion; and (5) the error in the proper motion difference is below 1.2 mas yr^{-1}.

For each of the cases where good astrometric quality was attained for our MSWD, sdB, or CV systems, we selected all stars with projected spatial separations less than 2×10^5 au from the system, and identified potential companions with good astrometric solution

Table 1. Ultrawide binarity/multiplicity fraction found in our research.

Type	Ultrawide multiplicity fraction	Uncertainty
MS + distant (A)	498/9934 ≈ 0.050	0.002
MS + distant (B)	197/2201 ≈ 0.089	0.006
$M_{\rm third} > 0.4\,M_\odot$		
MS + distant (B)	155/2201 ≈ 0.070	0.005
$M_{\rm third} > 0.6\,M_\odot$		
MS + distant (C)	161/3399 ≈ 0.047	0.004
sdB + distant	68/4709 ≈ 0.014	0.002
MSWD + distant no CEE	42/998 ≈ 0.042	0.006
pCE + distant	6/161 ≈ 0.037	0.015
CVs + distant	14/562 ≈ 0.025	0.007

and relative errors in parallax, and proper motions smaller than 0.33 of their value from the second *Gaia* data release. Following this step, we then considered whether these potential targets met the five criteria mentioned above.

We also made an additional check, as to reject a possible spurious origin of a wide companion due to association with a cluster. In particular, we searched for any known open clusters in the catalogue by Cantat-Gaudin et al. (2018) at angular separation of 1 deg with mean parallax difference of less than 0.3 mas and a mean proper motion difference of less than 2 mas yr^{-1}. Since this catalogue has no information about globular clusters, we also checked possible association to known globular clusters.

5 RESULTS

5.1 Comparison samples

In comparison sample A we identify 498 wide companions, from which we infer a multiplicity fraction of 5.0 ± 0.2 per cent (see Table 1). In order to estimate the contamination level, we then searched the positions of the same stars in the comparison sample but after shifting the locations by 1.0 deg in the declination direction (the largest size of the searching area for the sample), and performed the search again on this synthetic sample. In this case we find 103 ultrawide companions for the stars in the synthetic shifted sample (where 9 belong to the open cluster NGC 2632, which we therefore excluded). From these results we infer a chance alignment of companion stars at the level of 0.94 ± 0.1 per cent in our comparison sample.

In Fig. 1 we show the Hertzsprung Russel diagram for ultrawide components. The colour and magnitude data in this plot were corrected for reddening using the 3D map of Green et al. (2018). For the conversion of $E(B-V)$ to $A_{\rm g}$ and $E(B_{\rm p}-R_{\rm p})$ we use fixed values of $R = 3.1$, $A_{\rm g}/A_v = 0.9$ and $E(B_{\rm p}-R_{\rm p})/E(B-V) = 1.5$, and apply a factor of 0.884 to all the reddening values.

It seems that the stellar parameters determined by the Apsis algorithm indeed place primary stars at the main sequence just above the Sun and below an absolute magnitude of $G_{\rm abs} = 0$. The secondary stars are mostly low-mass stars with a mass distribution peaking at $M = 0.7\,{\rm M}_\odot$, see in Fig. 2.

The distribution of projected separations is shown in Fig. 3. In comparison to the work by El-Badry & Rix (2018) we extend the radius of the searching region up to 2×10^5 au and estimate the total ultrawide binarity fraction. It is also worth noting the following effect: in the *Gaia* DR2 two stars are considered as separate stars

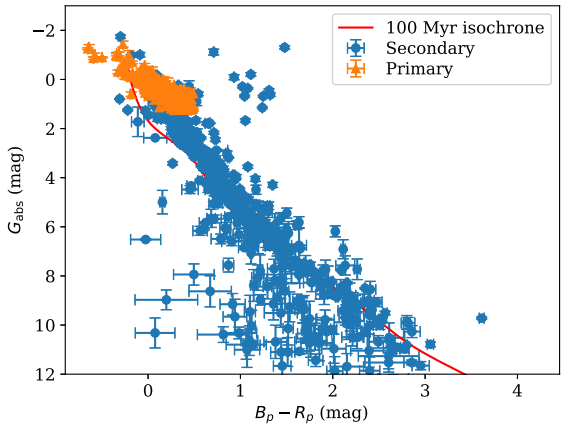

Figure 1. The Hertzsprung Russel diagram for ultrawide binaries found in comparison sample A.

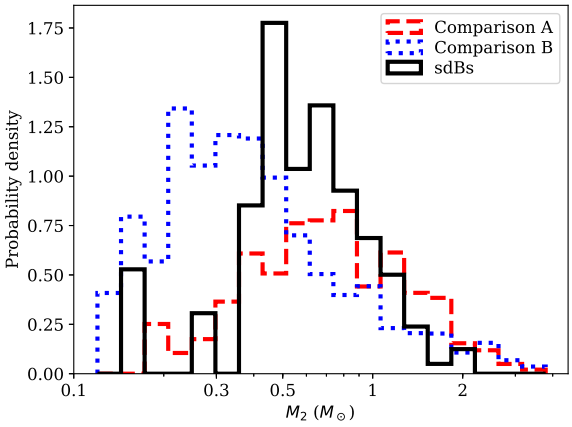

Figure 2. The distribution of masses of ultrawide companions for sdB stars and the comparison samples A and B.

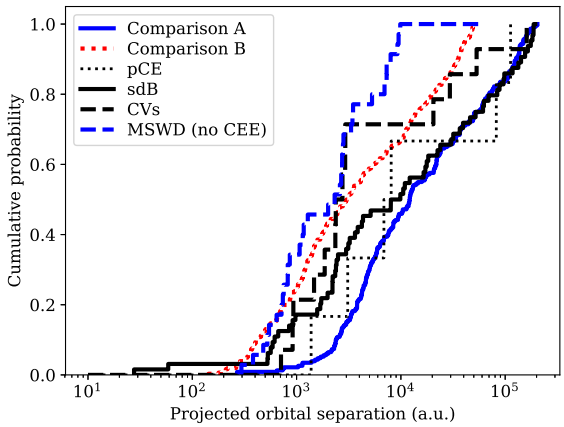

Figure 3. The cumulative distribution of orbital separations for the various post-CE systems and the comparison samples. Shown are ultrawide companions to sdB stars (solid black line), MSWD stars (dashed blue line; excluding close resolved binaries and ones with CEE) and short-period pCE-binaries (dotted black line), CVs (dashed black line), and the comparison samples A and B (excluding secondaries with masses less than 0.4 $M_\odot$).

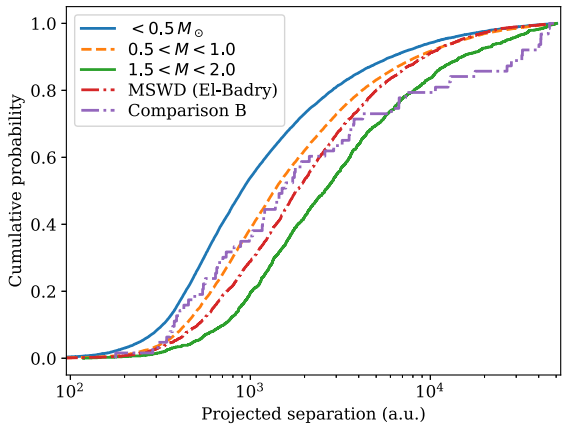

Figure 4. The cumulative distribution of projected separations to ultrawide companion (with a cut at $<5 \times 10^4$ au) for the sample of El-Badry & Rix (2018) and for the more massive stars from our comparison sample (this work).

with reliable photometry if the angular separation between them is more than 0.5–1 arcsec. It means that in the El-Badry & Rix (2018) sample the resolution is always better than 200 au. In our sample A most of the stars are located at typical distances of 1 kpc, and therefore the typical resolution is of the order of 1000 au.

In comparison sample B we initially identify 323 ultrawide binaries. We then excluded all systems with more than one ultrawide components as to get better resemblance to work by El-Badry & Rix (2018). Since this (B) comparison sample is of stars located much closer to us, it enables a better sensitivity to much fainter secondaries than in the sdBs sample (see Fig. 2). Therefore, we considered two additional cuts on the companion mass, in order to enable a proper comparison of the different sample. In particular, in one case we excluded all the systems where the secondary mass was less than 0.4 $M_\odot$ and in the second we considered a mass cut-off of 0.6 $M_\odot$. The results are summarized in Table 1. The distribution of the projected separations for sample B with the 0.4 $M_\odot$ cut-off is shown in Fig. 3.

Besides a shift in the cumulative distribution which could be caused by our limited resolution in comparison to El-Badry & Rix (2018), we see a clear trend for increasing projected separation of the ultrawide companion with increasing mass of the primary star, see Fig. 4.[3] We estimated the masses of the stars in the El-Badry & Rix (2018) sample using a combined isochrone (an age of 2 Myr for $M > 3.5\,M_\odot$, an age of 10 Myr for $1.8 < M < 3.5\,M_\odot$ and $M < 1.8\,M_\odot$ and an age of 0.5 Gyr[4]). When possible we corrected for absorption using Green et al. (2018). We find the difference between the cumulative distribution of MSWD ultrawide binaries and that of MSMS wide binaries to be smaller in comparison with the difference between the cumulative distribution of the projected separations for ultrawide components when the primary mass is less than 0.5 $M_\odot$ and the primary mass is in the range $1.5 < M < 2\,M_\odot$.

[3]This effect could be a consequence of the observational selection. More massive primaries tend to be further away and given a cut in distances they are more rare in the sample, so the sample becomes incomplete for projected separations of a few hundred AU.

[4]These ages are unimportant for the following analysis since we are mostly interested in the stellar mass at the zero age mass sequence and mass-loss is quite small for low-mass stars.

In the comparison sample C (massive primaries) we identify 297 ultrawide pairs. After we exclude repetitions and secondaries with masses less than 0.4 $M_\odot$ we are left with 180 objects. This results in a multiplicity fraction of 4.7 ± 0.4 per cent.

5.2 MSWD and PCE systems

In our analysis we have identified 63 common proper motions and parallax pairs to MSWD systems (see the distribution of the differences in position and proper motion in Fig. 5). It is worth noting that the SDSS spectroscope uses fibres with a diameter of 3 arcsec on the sky (York et al. 2000). Thereby, there is a number of binaries which are resolved in the *Gaia* data base (especially by the astro broad-band photometer with the angular resolution up to 0.1 arcsec), but are considered to be spectroscopic binaries in our MSWD sample. To deal with this problem we further divide our list into two parts. The common proper motion and parallax pairs with angular separations of less than 2 arcsec (21 pairs) are considered to be *resolved binaries*, see Table 2, while the 42 pairs with angular separations larger than 2 arcsec are considered to be *triples with ultrawide companion*, see Table 3. This division has a certain degree of arbitrariness, but it is impossible to make a better choice without additional observations. The third *Gaia* data release will provide information about the radial velocities and the binary properties which will help to better separate the samples.

We plot the projected orbital separations in Fig. 3. Six binaries which are marked as the post-common envelope systems in the catalogue seems to follow a much wider projected separation distribution than the general MSWD binaries which did not go through a CE episode. In particular, two systems with separations larger than 8×10^4 au are pCE binaries with third distant components.

We also plot the Hertzsprung Russel diagram for ultrawide components, see Fig. 6. We see that the majority of the ultrawide pairs are low-mass main sequence stars with spectral types G or K. Five objects are WDs, most of which are the components of the resolved binaries, supporting our original sample division. Two white dwarfs with colour $B_\mathrm{p} - R_\mathrm{p} \approx -0.1$ are well separated from the MSWD binaries (11 and 50 arcsec) which means that they are actual tertiary companions and not resolved MSWDs. For a large number of resolved binaries *Gaia* colours are not provided because the angular resolution of the medium-band photometers of the *Gaia* is 0.5–1 arcsec (Jordi et al. 2006) and the components of the binary are not resolved.

5.3 Hot subdwarf systems

In our sample we identify 68 ultrawide binaries for sdB stars, see Table 4, Fig. 7, and Table 1 for multiplicity fractions. It means that sdBs have 3.6 times smaller ultrawide multiplicity fraction than found in the comparison sample A which is located at similar distances. Another probe is a comparison with MSWD systems which did not go through the CEE. The ultrawide multiplicity fraction is three times smaller than in that sample. There is a small caveat in this comparison which we test in length in Appendix C; however we find it can only make up to 1.3 times difference between these fractions.

We plot the cumulative distribution of projected separations for ultrawide pairs to sdBs in Fig. 3. On average the ultrawide companions are located at larger distances than the ones found in the MSWD sample and at smaller distances than one found in comparison sample A. The probability for the distributions of projected orbital separations for the wide companions to sdBs and that of

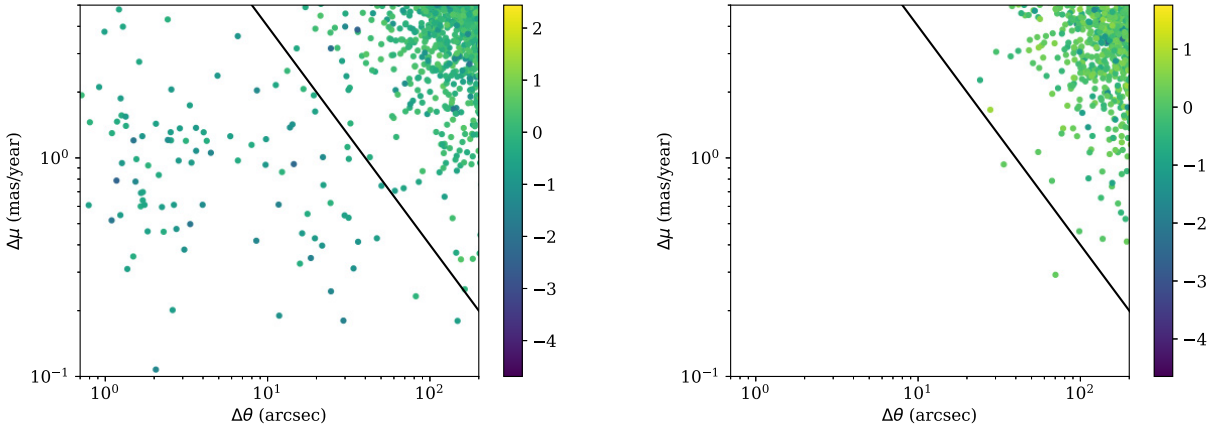

Figure 5. The difference in proper motions versus angular separations for MSWD systems. Left-hand panel: the real sample. Right-hand panel: the results for the mock, shifted sample (1.4 deg in the direction of right ascension). The colour shows the logarithm of the parallax difference. The black solid line guides the comparison between the real and the shifted samples.

Table 2. Resolved binaries found in the MSWD sample. *A* is the projected orbital separation.

Name	*Gaia* primary *Gaia* DR2 name	*Gaia* secondary *Gaia* DR2 name	$\Delta\theta$ (arcsec)	$\Delta\varpi \pm \sigma_{\Delta\varpi}$ (mas)	$\Delta\mu \pm \sigma_{\Delta\mu}$ (mas yr^{-1})	*A* (au)	pCE
SDSSJ011055.30-102011.9	2469937118135492480	2469937118136325632	1.7	0.188 ± 0.253	0.692 ± 0.381	234.1	N
SDSSJ024519.11+011157.3	2499299159543260928	2499299159545173760	1.7	0.505 ± 0.5	0.601 ± 0.734	761.1	N
SDSSJ025202.46-010515.7	2497494654803989760	2497494654805378816	1.7	0.303 ± 0.179	0.611 ± 0.276	985.1	N
SDSSJ081327.92+373245.6	907874108333645312	907874108334409856	0.8	0.789 ± 0.544	1.454 ± 1.177	472.9	N
SDSSJ084518.66+055911.7	583017522392120064	583017522392559232	1.3	0.368 ± 0.395	3.966 ± 1.186	352.2	N
SDSSJ091508.22+415559.5	816062001197670016	816062001196480256	1.7	0.114 ± 0.18	1.256 ± 0.241	441.8	N
SDSSJ092203.36+394002.0	812448078274747520	812448078276868096	1.5	0.045 ± 0.234	0.78 ± 0.283	357.1	N
SDSSJ103955.45+310643.5	736093077399500032	736093073107320192	1.7	0.381 ± 0.559	0.641 ± 0.716	225.7	N
SDSSJ105845.26+164714.9	3981879852457277440	3981879852457628416	1.5	0.013 ± 0.245	1.202 ± 0.521	523.4	N
SDSSJ111615.73+590509.3	857718476684324992	857718476683372288	1.1	0.015 ± 0.39	0.519 ± 0.857	428.4	N
SDSSJ112118.04+585036.4	857547532690379008	857547536985870592	1.4	0.23 ± 0.168	0.311 ± 0.272	692.4	N
SDSSJ114913.52-014728.6	3794340723954133504	3794340719659710720	1.7	0.307 ± 0.289	0.699 ± 0.367	336.2	N
SDSSJ131156.69+544455.8	1564508327957813632	1564508327956853888	1.3	0.155 ± 0.121	1.543 ± 0.184	307.2	N
SDSSJ134624.89+021734.2	3665130240625799808	3665130236330929792	1.2	0.181 ± 0.195	1.867 ± 0.333	248.9	N
SDSSJ135907.48+294209.3	1453655286472125440	1453655286473655680	1.8	0.762 ± 0.412	0.924 ± 0.644	323.2	N
SDSSJ152826.04+155916.4	1207541153468105344	1207541153466703872	1.5	0.569 ± 0.302	0.355 ± 0.398	791.4	N
SDSSJ155232.50+202715.3	1204454485026467200	1204454485024334720	0.9	0.252 ± 0.285	2.104 ± 0.341	259.8	N
SDSSJ155735.37+155817.2	1193136971322193792	1193136971325031296	1.2	0.004 ± 0.447	0.788 ± 0.516	695.7	N
SDSSJ170127.36+253302.6	4573134327556676224	4573134323259272064	1.8	0.26 ± 0.131	0.462 ± 0.191	396.2	N
SDSSJ172439.05+551600.1	1419718383339799168	1419718379044501632	1.2	0.18 ± 0.283	0.548 ± 0.592	746.7	N
SDSSJ233919.64-000233.4	2642852260954014848	2642852260954740480	1.1	0.542 ± 0.476	1.297 ± 0.702	258.8	N

MSWDs (i.e. triples) are similar is 2.4×10^{-5} according to the Kolmogorov−Smirnov (KS) test. The probability that the projected separations for the ultrawide companions in the comparison sample A (i.e. binaries) and that of the sdBs are drawn from the same distribution is 6×10^{-3} according to the KS test.

We also estimated the chance alignment contamination. In order to do so, we shifted the position of each sdB star in the catalogue by 1.4 deg in declination. We then performed the search for ultrawide binaries using these synthetic positions. We found eight pairs, two of them paired with the actual host, as it turned out that a few stars are located closer than $\varpi = 10$ and the shift of 1.4 deg is not sufficient to exclude them from the search region. Therefore, the chance alignment contamination is $6/4709 \approx 0.0013 \pm 0.0005$; this value is ten times smaller than the detected ultrawide multiplicity for sdBs, affirming that the detected wide companions are likely genuine and are not the result of background contamination.

As an additional check we searched Table 4 and checked the literature for known close companions for any of these objects. Our original list contained six more objects which were excluded as we briefly discuss below.

ζ^1 Cnc A (Roman 1950; Abt 1981) is a known resolved binary with an sdB component which we also found in the *Gaia*.

BD-12134A is known to be hierarchical triple at the centre of the planetary nebula NGC 246 (Adam & Mugrauer 2014). BD-12134C is located at separation of ≈1 arcsec from the BD-12134A. In our analysis we could not identify it since star is very red and faint with $J \approx 18.4$.

The system CD-229142 was suspected to be a binary (Stys et al. 2000), the *Gaia* search turned out an additional component to this system.

CD-4214462 seems to be a binary with spectroscopically identified white dwarf (McCook & Sion 1999).

CPD-73420 is known to be a binary star (Zacharias et al. 2012).

Table 3. Wide binaries found in the MSWD sample. A is the projected orbital separation.

Name	*Gaia* primary *Gaia* DR2 name	*Gaia* secondary *Gaia* DR2 name	$\Delta\theta$ (arcsec)	$\Delta\varpi \pm \sigma_{\Delta\varpi}$ (mas)	$\Delta\mu \pm \sigma_{\Delta\mu}$ (mas yr^{-1})	A (au)	pCE
SDSSJ002428.44-102443.5	2424897475435562368	2424897479729961984	4.0	0.059 ± 0.412	0.611 ± 0.477	1281.2	N
SDSSJ014246.00-094731.0	2464385576553809792	2464385580847869952	2.8	0.152 ± 0.419	0.972 ± 0.654	643.4	N
SDSSJ022615.69-010423.9	2499922071535617280	2499922067240455168	6.5	0.501 ± 0.357	0.973 ± 0.553	2730.4	N
SDSSJ023650.60-010313.3	2497111028324980736	2497111097044458880	21.9	0.257 ± 0.302	0.752 ± 0.451	9503.0	N
SDSSJ024642.55+004137.2	2499031084864744448	2499031192239169280	18.3	0.029 ± 0.195	0.35 ± 0.317	6875.4	Y
SDSSJ030607.18-003114.4	3266296412128039424	3266279026100283008	778.2	0.124 ± 0.089	0.319 ± 0.121	112642.6	Y
SDSSJ030716.44+384822.8	142664833456549120	142664833456549376	3.6	0.085 ± 0.195	1.077 ± 0.22	1378.4	Y
SDSSJ032510.84-011114.1	3262517837340737152	3262517841635204608	2.9	0.205 ± 0.119	1.364 ± 0.218	295.8	N
SDSSJ080120.47+064614.7	3144220281799428736	3144220286094183680	3.3	0.013 ± 0.19	0.499 ± 0.2	822.6	N
SDSSJ081647.38+534017.8	1031806794114311552	1031806798409670016	11.7	0.076 ± 0.139	0.191 ± 0.195	3328.7	N
SDSSJ082823.55+470001.3	930577850922831616	930577855217008000	4.5	0.04 ± 0.161	1.055 ± 0.229	717.3	N
SDSSJ085426.25+374653.0	719483236276555008	719483236276554880	2.6	0.164 ± 0.173	0.611 ± 0.234	479.0	N
SDSSJ091218.46+150334.4	607478387644308736	607478391935326848	2.1	0.423 ± 0.378	0.835 ± 0.506	752.2	N
SDSSJ093809.28+143037.0	617887567299257600	617887567299258752	11.2	0.369 ± 0.393	2.149 ± 0.457	2676.9	N
SDSSJ095756.81+361444.9	796612911812751616	796612843095588736	2.0	0.226 ± 0.435	1.431 ± 0.524	382.1	N
SDSSJ101958.61+283339.8	741061353833562880	741061353833562368	24.4	0.038 ± 0.371	0.246 ± 0.544	7299.7	N
SDSSJ102118.15+265101.1	728746686163222272	728746686163197440	9.7	0.118 ± 0.259	0.93 ± 0.257	2315.9	N
SDSSJ104959.80-004719.0	3803142859993965952	3803142829929703552	14.4	0.006 ± 0.173	0.937 ± 0.287	2783.4	N
SDSSJ105607.54+583943.3	860485462121503360	860485466415271680	2.2	0.188 ± 0.254	0.597 ± 0.323	822.7	N
SDSSJ105806.04+152225.9	3969333600151218176	3969333600151218304	8.5	0.04 ± 0.12	0.419 ± 0.182	5288.5	N
SDSSJ111046.29+612225.2	861984959757517184	861984955461732992	29.1	0.027 ± 0.223	0.181 ± 0.38	9858.0	N
SDSSJ114716.07+293930.3	4020741021494570624	4020741025789617536	31.3	0.286 ± 0.297	0.533 ± 0.45	9271.6	N
SDSSJ115553.94+105255.2	3918510771102102528	3918510839821579392	21.5	0.109 ± 0.166	0.398 ± 0.164	7970.8	N
SDSSJ115848.87+171553.1	3926599225312457472	3926599122233242112	33.5	0.087 ± 0.226	0.313 ± 0.348	7300.9	N
SDSSJ124808.93+605726.4	1579901250228323584	1579901250228323712	2.6	0.195 ± 0.123	0.202 ± 0.172	738.2	N
SDSSJ124959.75+035726.6	3705361680324471424	3705362504958192512	146.0	0.204 ± 0.108	0.181 ± 0.153	59698.3	N
SDSSJ142149.14+382833.3	1484715149927519104	1484715154222882176	3.3	0.244 ± 0.308	1.736 ± 0.511	544.3	N
SDSSJ142951.19+575949.0	1611769731470117120	1611769735766328576	16.2	0.161 ± 0.16	0.453 ± 0.276	8071.5	Y
SDSSJ143642.01+574146.3	1611031615570789760	1611034334286174080	324.6	0.117 ± 0.127	0.248 ± 0.229	82181.7	Y
SDSSJ145248.79+234807.6	1266149972245838720	1266149972245864576	5.9	0.213 ± 0.292	1.255 ± 0.52	2813.7	N
SDSSJ145642.71+053101.8	1159963910942567168	1159963983957684736	21.7	0.052 ± 0.18	1.008 ± 0.327	3432.3	N
SDSSJ153009.49+384439.8	1387898512537120768	1387898516831996544	4.0	0.28 ± 0.192	1.309 ± 0.311	2005.6	N
SDSSJ154843.79+372749.7	1376105769292093184	1376105739228731392	19.4	0.148 ± 0.136	0.43 ± 0.274	3091.6	Y
SDSSJ162020.89+214542.9	1298515020427786624	1298515024723278336	2.0	0.041 ± 0.159	0.108 ± 0.244	524.8	N
SDSSJ170546.61+274028.3	4574942916809993088	4574942916808430336	2.5	0.187 ± 0.393	1.31 ± 0.599	860.9	N
SDSSJ173430.11+335407.5	4602418200558831232	4602418204854379520	3.6	0.161 ± 0.223	1.371 ± 0.451	1069.7	N
SDSSJ192306.01+620310.7	2240323111314621056	2240323111318292096	3.4	0.168 ± 0.316	0.951 ± 0.603	2602.3	N
SDSSJ192616.13+383400.8	2052736600737294336	2052736600733320448	3.1	0.078 ± 0.219	0.382 ± 0.419	1144.8	N
SDSSJ204713.67+002203.8	4228388774562523264	4228388602763827584	49.8	0.187 ± 0.257	0.746 ± 0.319	6967.9	N
SDSSJ213225.96+001430.5	2687732916851442304	2687733015641916544	2.4	0.073 ± 0.49	1.207 ± 0.911	1170.5	N
SDSSJ230202.49-000930.0	2651675425155232128	2651675051493595392	14.1	0.093 ± 0.246	1.421 ± 0.248	3479.1	N
SDSSJ233919.64-000233.4	2642852260954014848	2642852329674217088	11.6	0.031 ± 0.228	0.612 ± 0.366	2733.4	N

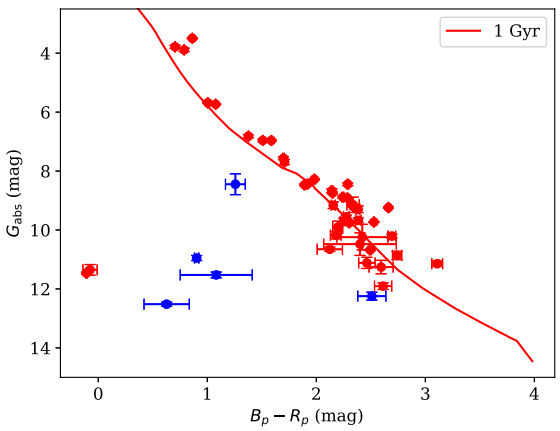

Figure 6. The Hertzsprung Russell diagram for the third (red dots) and the second (blue dots) components of MSWD systems.

EC21494-7018 might have an extremely low-mass white dwarf companion according to Vennes et al. (2015).

HD136176B and HD166370B are known to be visually resolved binaries (Gili & Bonneau 2001; Gontcharov 2012).

PG0834+501 shows variations of radial velocity with amplitude ≈50 km/s (Saffer, Livio & Yungelson 1998; Good et al. 2005).

TYC6347-931-1 is known to have a visually resolved companion according to the Simbad data base

V∗AHMen is an accreting WD emitting X-ray (Wood et al. 1984; Mukai 2017).

V∗TXCol is an intermediate polar (Tuohy et al. 1986; Suleimanov, Doroshenko & Werner 2019) with an orbital period of ≈5.7 h.

Additionally we noticed that some of sdBs stars actually belong to the globular cluster NGC 6752. In this case multiple stars could be seen as ultrawide pairs, therefore we removed these objects

Table 4. The identified sdB systems with wide companions. *A* is the projected orbital separation. The information about any known multiplicity of the sdB star is provided in Mult. column. with several possible options; Yes – known binarity of the sdB, No – no information, Known – the found companion is known. Question mark means what existence of binary component is not confirmed with certainty.

Name	*Gaia* primary *Gaia* DR2 name	*Gaia* secondary *Gaia* DR2 name	$\Delta\theta$ (arcsec)	$\Delta\varpi \pm \sigma_{\Delta\varpi}$ (mas)	$\Delta\mu \pm \sigma_{\Delta\mu}$ (mas yr^{-1})	A (au)	Mult.
zet01CncA	657244521593509376	657244586015485440	1.1	0.339 ± 0.237	64.592 ± 0.374	27.6	Known
2MASSJ01531776+3542049	330261789400007040	330264916136195072	92.0	0.226 ± 0.379	0.129 ± 0.76	83948.3	No
2MASSJ08251803+1131062	601188910547673728	601188910547673600	2.7	0.114 ± 0.071	0.139 ± 0.116	3856.5	No
BD-12134A	2376592910265354368	2376592910265354496	3.9	0.153 ± 0.106	0.383 ± 0.22	1982.9	Known
BPSBS17579-0012	2550973079312403712	2550973083608089984	2.7	0.104 ± 0.07	0.432 ± 0.113	1686.6	No
CD-229142	3492203484216217856	3492203484216217728	7.6	0.057 ± 0.088	0.605 ± 0.09	2209.0	Known
CD-4214462	6688624794231054976	6688624794233492864	6.9	0.16 ± 0.17	1.206 ± 0.234	916.1	Yes
CPD-73420	5262163664424670848	5262163664426978816	1.7	0.026 ± 0.046	0.659 ± 0.093	529.9	Known
EC05015-2831	4877263019073081600	4877263023370516096	20.9	0.13 ± 0.081	0.334 ± 0.134	12146.6	No
EC21494-7018	6395639996658760832	6395639923642870272	15.4	0.316 ± 0.52	1.231 ± 0.725	3132.3	Yes?
FBS0638+428	963881581386403072	963881577091962368	3.8	0.284 ± 0.308	0.57 ± 0.444	3233.5	No
Feige91	1660055029417965952	1660055098137442944	39.8	0.074 ± 0.102	0.441 ± 0.165	18292.1	No
GALEXJ063952.0+515658	992534888766785024	992534888766784640	7.0	0.1 ± 0.075	0.17 ± 0.135	2384.9	No
GALEXJ110055.9+105542	3868418219635118080	3868418219635275520	8.6	0.332 ± 0.172	0.098 ± 0.458	8019.4	No
HD136176B	1271209615518148736	1271209611223823232	1.6	0.059 ± 0.066	11.352 ± 0.081	58.8	Known
HD137737	5820064282494545280	5820064282512073728	2.7	0.101 ± 0.069	0.468 ± 0.104	2208.9	No
HD166370B	6726045641698117888	6726045641691326976	2.0	0.015 ± 0.124	1.136 ± 0.306	847.1	Known
KPD2254+5444	2002880555945732992	2002880555945731968	3.4	0.032 ± 0.085	0.284 ± 0.131	2347.0	No
M27	1827256624493300096	1827256628817680896	6.4	0.067 ± 0.062	0.303 ± 0.086	2417.0	No
NGC 675250	6638380690556259072	6638376567387480704	244.0	0.096 ± 0.435	0.077 ± 0.495	182602.9	No
–	364729314267240192	364729314267239936	9.2	0.066 ± 0.13	0.206 ± 0.208	10911.3	–
–	340170996210473856	340171000507010176	2.2	0.034 ± 0.196	0.183 ± 0.225	1575.4	–
–	170774775937432832	170774879016640000	61.3	0.394 ± 0.294	0.079 ± 0.498	88246.9	–
–	3009110712427319296	3009110716723715840	42.1	0.059 ± 0.07	0.094 ± 0.13	46036.1	–
–	3342874205845523072	3342874240205256704	38.1	0.062 ± 0.059	0.197 ± 0.088	16508.8	–
–	196726961201325568	196726961201325184	4.2	0.104 ± 0.105	0.461 ± 0.16	2982.7	–
–	5280973147283545344	5280973525240620928	136.3	0.005 ± 0.04	0.237 ± 0.072	61316.1	–
–	5614913348547819392	5614913211099174656	120.2	0.336 ± 0.232	0.061 ± 0.398	96390.8	–
–	690626278727938304	690626278727938560	2.4	0.065 ± 0.066	0.126 ± 0.053	2495.0	–
–	5355946268217174656	5355946268217174400	4.3	0.015 ± 0.033	0.095 ± 0.059	4334.6	–
–	5198534239334516992	5198534204974777984	19.1	0.03 ± 0.064	0.162 ± 0.112	17173.0	–
–	5856360741911875840	5856360776271617024	26.7	0.218 ± 0.142	0.049 ± 0.23	36687.5	–
–	6083515098240961920	6083515858449657344	191.9	0.2 ± 0.479	0.069 ± 0.635	133618.3	–
–	5899284885568130560	5899284881258356864	30.4	0.775 ± 0.402	0.312 ± 0.782	30377.7	–
–	5903913348492755072	5903916333476091264	110.7	0.434 ± 0.233	0.083 ± 0.44	165034.5	–
–	5983018743361688064	5983018743361687424	2.3	0.055 ± 0.078	0.102 ± 0.127	2216.6	–
–	5981257806743601792	5981257909822816256	42.3	0.033 ± 0.11	0.55 ± 0.243	17692.2	–
–	5832927778318780416	5832927640879800064	97.5	0.302 ± 0.183	0.031 ± 0.251	117800.1	–
–	5938577715980303616	5938578510554279552	167.8	0.371 ± 0.426	0.115 ± 0.768	186934.0	–
–	4112632469609705472	4112632469562573568	1.3	0.089 ± 0.116	0.799 ± 0.27	974.9	–
–	5918752941519223424	5918752941519228288	26.6	0.018 ± 0.081	0.236 ± 0.14	22451.8	–
–	4501644012800425216	4501644012800888320	4.5	0.078 ± 0.08	0.041 ± 0.14	4229.8	–
–	6709698863028116096	6709698863028118528	8.2	0.036 ± 0.087	0.42 ± 0.131	5127.4	–
–	4085168799440497792	4085168593282058368	47.5	0.082 ± 0.082	0.054 ± 0.138	52037.3	–
–	6632375639082824064	6632375673442542720	59.9	0.345 ± 0.223	0.128 ± 0.246	62553.0	–
–	6632375639082824064	6632372237462530048	136.0	0.874 ± 0.464	0.051 ± 0.524	141949.5	–
–	6632375639082824064	6632375501638566912	179.7	0.474 ± 0.393	0.082 ± 0.444	187551.0	–
–	4301614775823709568	4301614737148533504	29.7	0.108 ± 0.258	0.152 ± 0.433	39432.0	–
–	1821561467841789312	1821561467841789056	2.7	0.103 ± 0.057	0.151 ± 0.07	3629.3	–
–	2035560412373115648	2035566558436603392	261.3	0.091 ± 0.283	0.075 ± 0.447	194292.8	–
–	4299127989744823424	4299128058464308096	25.0	0.012 ± 0.061	0.142 ± 0.085	9876.4	–
–	2686841281644006656	2686841071191184512	81.6	0.124 ± 0.142	0.064 ± 0.173	69282.1	–
–	2686841281644006656	2686850386972924544	182.8	0.345 ± 0.254	0.039 ± 0.345	155168.3	–
–	2208678999172871424	2208678999172872704	10.8	0.025 ± 0.033	0.068 ± 0.052	7995.8	–
–	1925448205463385344	1925448205467420160	1.2	0.215 ± 0.184	1.136 ± 0.247	666.8	–
PG0834+501	1027028630113289600	1027028625817982976	44.6	0.259 ± 0.278	0.319 ± 0.308	23857.3	Yes
PNA6633	3827045525522912128	3827044765316735104	1.8	0.095 ± 0.108	0.282 ± 0.196	1723.6	No
PNA6634	5690534730341025408	5690534734636923520	9.1	0.025 ± 0.108	0.231 ± 0.203	10527.4	No
TYC2650-973-2	2093326416800046848	2093326416802711680	1.4	0.081 ± 0.072	1.52 ± 0.144	525.9	No
TYC3533-2439-1	2122270063965861504	2122269960886645760	46.0	0.027 ± 0.059	0.073 ± 0.104	31778.1	No
TYC4213-1610-1	2161688071217417728	2161688071217418240	3.6	0.021 ± 0.033	1.054 ± 0.069	615.7	No
TYC4454-1229-1	2251716426898467200	2251716426895634560	1.9	0.041 ± 0.093	0.922 ± 0.205	565.3	No
TYC6347-931-1	6884185998227170304	6884185998226359552	1.0	0.193 ± 0.116	0.433 ± 0.15	589.1	Known
V∗MMCrA	4035877654477649152	4035877933682412928	181.2	0.387 ± 0.372	0.01 ± 0.463	176067.8	No

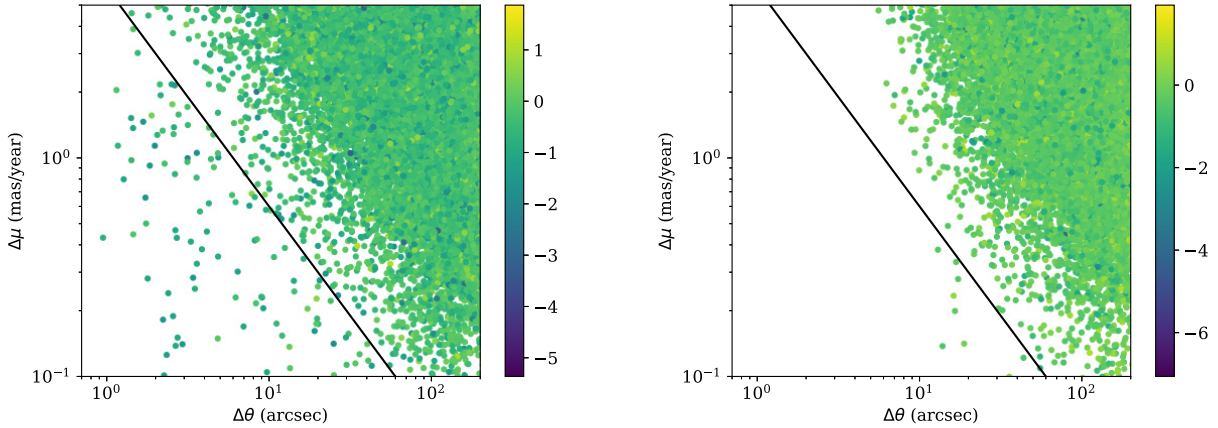

Figure 7. The difference in proper motions versus angular separations for sdBs. Left-hand panel: the actual sample. Right-hand panel: all the objects are shifted by 1.4 deg in the direction of right ascension as to exclude any possible real wide binaries from the mock-sample. The colour shows the logarithm of the parallax difference. The black solid line assists comparison between the misplaced and observed sample.

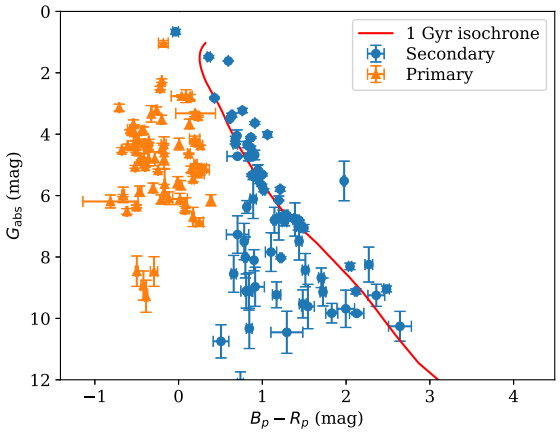

Figure 8. The Hertzsprung Russell diagram for ultrawide companions to sdBs.

from our list. Also V∗AHMen and V∗TXCol are already present in our list of CVs and therefore we excluded them from the sdB list.

Following the prescription from the previous section we have similarly prepared the Hertzsprung Russell diagram for the primary sdB stars and their ultrawide companions (see Fig. 8). The companions seems to be normal typical low-mass main sequence stars. We notice that four primary systems lay close to the top of the white dwarf sequence ($G_{abs} \approx 9$ and $B_p - R_p \approx -0.5$) and, therefore, they might in fact be white dwarf and not sdB stars. We therefore excluded the following potential contaminants to the sdB sample: *Gaia* DR2 1605126585296788480, 5957303154940605696, 2MASSJ14360144+5227424, and *Gaia* DR2 2867830997336128256.

It is worth noticing that the distribution of projected separations for the ultrawide companions of MSWD binaries sample is skewed towards smaller separations in comparison with the sdB sample (see Fig. 3). We believe that this effect occurs because the MSWD are composed of low-mass stars with long time-scale of mass ejection (AGB stage) while sdBs are more massive stars with possible fast mass ejection. The fast mass ejection unbinds many utrawide systems. Systems which survive fast mass ejections tend to be wider than ones surviving slower mass ejection.

We also test whether the difference in projected separations between the sdB sample and the comparison sample A is caused by some observation selection effect or whether it is a real effect. To do so we plot the companion absolute magnitude versus projected separation for both samples in Fig. 9 (left-hand panel). We see that sdB's companions cover the same range of projected separations as companions to stars from the A sample with an exception of two known close-by companions to the stars zet01 Cnc and HD136176B.

If we compare the MSWD sample with sdBs in a similar Fig. 9 (right-hand panel), we notice that the companions to MSWDs are more concentrated towards the fainter side, an aspect which might be partly explained by the smaller masses of the MSWDs in comparison to the sdBs progenitors.

5.3.1 Distance-parallax conversion

Before discussing the final results it is also important to verify whether the projected separations we find are physical and are not affected by some sort of a bias. A potential problem could arise from the direct conversion from distance to parallax.

The conversion from parallax to distance is not straightforward when the accuracy of the parallax measurement is limited (Bailer-Jones 2015; Igoshev, Verbunt & Cator 2016; Bailer-Jones et al. 2018). To check the contribution of this effect we collect the Bayesian estimates for distances using the catalogue of Bailer-Jones et al. (2018) and plot the cumulative distributions of projected separations in Fig. 10. We find the difference to be negligible.

5.4 Cataclysmic variables

We found 14 ultrawide pairs to cataclysmic variables, see Table 5. The distribution of the projected separations is shown in Fig. 3. Half of objects (mostly type NL) are found to have projected separations concentrated around a few $\times 10^3$ au, another half (mostly DN) are concentrated at larger separations of a few $\times 10^4$ with the largest separation of J0221+7322 at $\approx 1.6 \times 10^5$ au. The multiplicity fraction is two times smaller than the multiplicity fraction found for comparison sample C, see Table 1. A smaller multiplicity fraction hints that the systems experienced a more significant mass-loss episode.

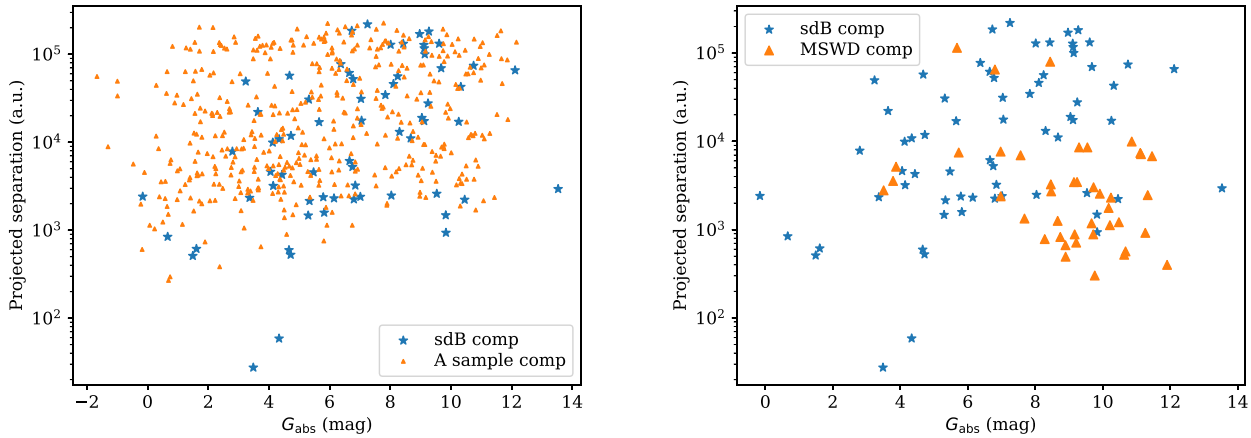

Figure 9. Projected separation of the ultrawide companions as a function of their absolute magnitude for stars in the A sample (left-hand panel) and the MSWD (right-hand panel).

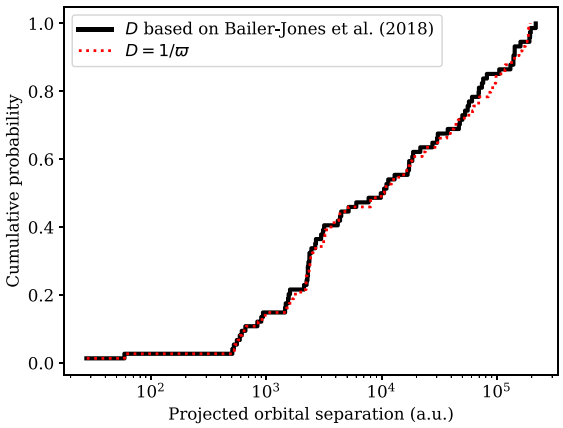

Figure 10. The distribution of projected separations for ultrawide companions to sdB stars derived using $D = 1/\varpi$ (dashed, red line) and the Bayesian estimate for distance based on work by Bailer-Jones et al. (2018) (black, solid line).

Note that one might argue that the comparison of sample C with CVs is invalid, since sample C consists of ultrawide binaries while CVs with distant companions are in fact triples so their multiplicity fraction might be irrelevant for the comparison. This argument does not seem to be valid because the fraction of CVs with distant companion (2.5 per cent) is also smaller in comparison to the fraction of MSWD stars with distant ultrawide companion (i.e. triples) which did not go through a common envelope episode.

6 SIMULATIONS OF ORBITAL EVOLUTION FOR SYSTEMS WITH COMMON ENVELOPE EJECTION

In the previous section we demonstrated that the multiplicity fraction for systems which likely went through a CEE is typically 2–4 times smaller than the fractions in the corresponding comparison samples A, B, C, or among systems which did not go through the CEE. In this section we perform gravitational dynamics simulations of hierarchical triples where we include mass-loss from the inner binary in order to estimate the probability for a system to survive the CE ejection episode. We then compare the resulting projected separations with the ones found in the previous section.

6.1 Method

In our simulations we make a simplified calculation where we replace the primary star in the appropriate comparison sample with a progenitor binary at the CE stage that loses mass at some given rate, where different mass-loss rates are considered as to identify the mass-loss rate that best reproduces the observations. We then follow the evolution of that star and its wide companion, as to synthesize a post-CE-like system with a wide companion that lose mass through the CEE. We follow the evolution of the orbital elements of a distant companion depending on mass-loss rate.

In order to perform the simulations we use a technique similar to the one described in Michaely & Perets (2019) with a small difference. Namely, we consider a ultrawide binary to be unbound if its orbital energy is positive or its projected separation exceeds the size of our searching region i.e. 2×10^5 au.

The initial parameters for our simulations are as follows. First, we select ultrawide binaries from the comparison sample. Then, we consider five random eccentricities for each binary sampled from a thermal eccentricity distribution (Ambartsumian 1937; Heggie 1975) and five eccentric anomalies from a uniform distribution. While the eccentricity distribution of solar-type binaries is uniform (Raghavan et al. 2010), the eccentricity distribution of very wide companions is somewhat similar to thermal (Tokovinin & Kiyaeva 2016; Moe & Di Stefano 2017). We take the semimajor axis to be 1.02 of the observed projected separation based on the analysis by Dupuy & Liu (2011).

We assume that the CE ejection starts immediately at the beginning of the simulation. The orbital motion of the system is integrated using the Hermite fourth-order integration scheme with addition of a jerk force due to the mass-loss (Hut, Makino & McMillan 1995). The numerical integration continues until the CE ejection is finished i.e. the primary mass reaches $M_{\rm final}$. We convert the final masses, orbital positions, and velocities into new semimajor axis a_f, eccentricity e_f, and eccentric anomaly. The final average separation is then computed as:

$$s_f = a_f \left(1 + \frac{1}{2} e_f^2\right). \quad (1)$$

We assume that a binary stays bound after the CE ejection if $s_f < 2 \times 10^5$ au and $e_f < 1$.

As we discuss below, each type of system has a different typical total mass-loss, depending on the progenitors and final remnants,

Table 5. Wide binaries found in the CVs sample. *A* is the projected orbital separation. Types are DN – dwarf novae, NL – nova like variable, CV – general CV.

Name	*Gaia* primary *Gaia* DR2 name	*Gaia* secondary *Gaia* DR2 name	$\Delta\theta$ (arcsec)	$\Delta\varpi \pm \sigma_{\Delta\varpi}$ (mas)	$\Delta\mu \pm \sigma_{\Delta\mu}$ (mas yr^{-1})	A (au)	Type
0218+3229	325051822271077376	325051817976249600	5.7	0.194 ± 0.343	0.538 ± 0.647	2930.3	DN
AH Men	5207385651533430912	5207384891323130368	2.9	0.033 ± 0.024	0.141 ± 0.046	1470.5	NL
AY Psc	2565601982736199168	2565601982736199296	39.4	0.09 ± 0.12	0.192 ± 0.198	29489.7	DN
J0154-5947	4714563374364671872	4714563168206242048	8.5	0.015 ± 0.046	0.42 ± 0.076	2753.3	NL
J0221+7322	546910213373341184	546916569924806272	465.5	0.329 ± 0.422	0.113 ± 0.768	160856.5	DN
J0800+1924	670132550216853632	670132545920724224	3.4	0.666 ± 0.391	0.331 ± 0.475	2352.7	DN
J1930+0530	4294249387962232576	4294249387935557888	2.2	0.102 ± 0.092	1.395 ± 0.252	708.9	CV
J2256+5954	2014349389931360768	2014349389931359616	5.9	0.034 ± 0.029	0.408 ± 0.041	2922.3	NL
MR UMa	772038105376131456	772038105376626432	5.5	0.15 ± 0.175	0.423 ± 0.231	1860.5	DN
NGC 104-W1	4689639301203677952	4689639232475726976	39.2	0.163 ± 0.383	0.229 ± 0.519	20498.7	CV
NY Lup	5988071549046301184	5988071579074013824	41.8	0.121 ± 0.165	0.055 ± 0.269	53197.5	NL
TX Col	4804695427734393472	4804695423438691200	2.6	0.07 ± 0.044	0.19 ± 0.087	2374.8	NL
V3885 Sgr	6688624794231054976	6688624794233492864	6.9	0.16 ± 0.17	1.206 ± 0.234	916.1	NL
V453 Nor	5984221987022142464	5984221987004209920	3.2	0.189 ± 0.507	1.492 ± 0.968	931.1	DN

and we therefore discuss the simulations results for each type of system individually.

6.2 Hot subdwarf systems

We perform the simulations considering two possible final masses; either assuming $M_{\rm final} = 0.9\,M_\odot$ or $M_{\rm final} = 0.4\,M_\odot$. We also consider both a constant mass-loss rate and an exponentially decaying mass-loss rate in form:

$$M(t) = M_0 \exp(-t\tau), \quad (2)$$

where M_0 is the initial mass of the inner binary and τ is an inverted time-scale. The initial progenitor masses for sdB are between 2.5 and 4 $M_\odot$ (and taken accordingly from samples A and B). Our motivation to choose such massive progenitors is based on study by Han et al. (2002), Han et al. (2003) who suggested that majority of sdB stars are formed from primaries less massive than 3 $M_\odot$. The addition of some secondary mass gives us the mentioned upper limit. The final mass could be as small as a mass of a single sdB i.e. $\approx 0.4\,M_\odot$ or an sdB with some low-mass companion i.e. $0.9\,M_\odot$. We use two samples to simulate the sdBs: (1) using our sample A and (2) using the closer-by systems in sample B.

Using sample A we fail to reproduce the sdBs with ultrawide companion at separations of 2–4 $\times$ 10^3 au, see Fig. 11. We believe this results from the omission of smaller separation systems that cannot be resolved in sample A. In particular, systems with 0.5–1 $\times$ 10^3 au separations which are below the *Gaia* resolution for stars located at distances of $\approx$1 kpc. Following mass-loss these systems would have widened and fill in the smaller separation regime in the separation distribution. Since these systems are undersampled in sample A, the resulting simulated systems show a depletion in systems with small separations. In Fig. 11 we scaled the cumulative probability down as to normalize it to the total survival probability computed for the whole sample. Additionally we show the results of our simulations with exponentially decaying mass-loss rates in right-hand panel of Fig. 11.

In order to overcome the potential problem we performed the same study, but used sample B. This sample of close-by systems better samples even smaller separation systems.

Using sample B we were able to reproduce the ultrawide companions at separations of 2–4 $\times$ 10^3 au, see Fig. 12. Note, however, that in this case we cannot normalize the distribution properly. The close-by stars sample is more sensitive to the detection of fainter companions (below $\sim 0.5\,M_\odot$), and therefore cannot be directly compared with the large *Gaia* sample of sdBs. Nevertheless, if we set a lower limit of $0.4\,M_\odot$ for the companion we can decrease the ultrawide binarity fraction and effectively produce a better comparison; in this case the fraction reduced from $\approx$11 per cent to $\approx$9 per cent. Even if a larger fraction of sdBs have light ultrawide binary companions, they are impossible to discover with *Gaia* at the moment.

Overall, we are able to reproduce the multiplicity of the ultrawide companions and the distribution of their projected separations only if the CE ejection time-scale is compatible with short ejection time-scales i.e. $\dot{M} \gtrsim 10^{-2}\,M_\odot\,{\rm yr}^{-1}$. We also tested this by performing additional simplified simulations where the orbital elements were computed using the equation from Hills (1983).

6.3 Cataclysmic variables

For this simulations we use sample C which includes primary stars with masses in the range 3.5−9 $M_\odot$ and the distant companions with masses larger than $0.4\,M_\odot$. We assume the final mass of the inner binary to be $1.8\,M_\odot$ i.e. there is $\approx 1\,M_\odot$ CO WD and $\approx 0.8\,M_\odot$ secondary star.

The results of our simulations are shown in Fig. 13. The small number of CVs with ultrawide companion is strongly limiting the possibility of a good detailed comparison, and therefore the overall multiplicity fraction is the main indicator for a successful reproduction of the observations. In order to reproduce the observed fraction we find that a longer CE ejection time-scale of $\dot{M} \approx 10^{-4}\,M_\odot\,{\rm yr}^{-1}$ is required (i.e. a total mass-loss time-scale of a few $\times 10^4$ yr is required, given the massive progenitors.

7 DISCUSSION AND SUMMARY

We find that the distributions of projected separations of post-CE systems with additional wide-companions differ significantly from the distribution of projected separation for ultrawide companions to corresponding possible progenitor stars in systems which did not go through a CE evolution. We suggest that this can be attributed to the envelope ejection during an episode of CE evolution. In this case the difference in the distributions can be used to constrain the CE process, and in particular the time-scale for mass-loss during this process.

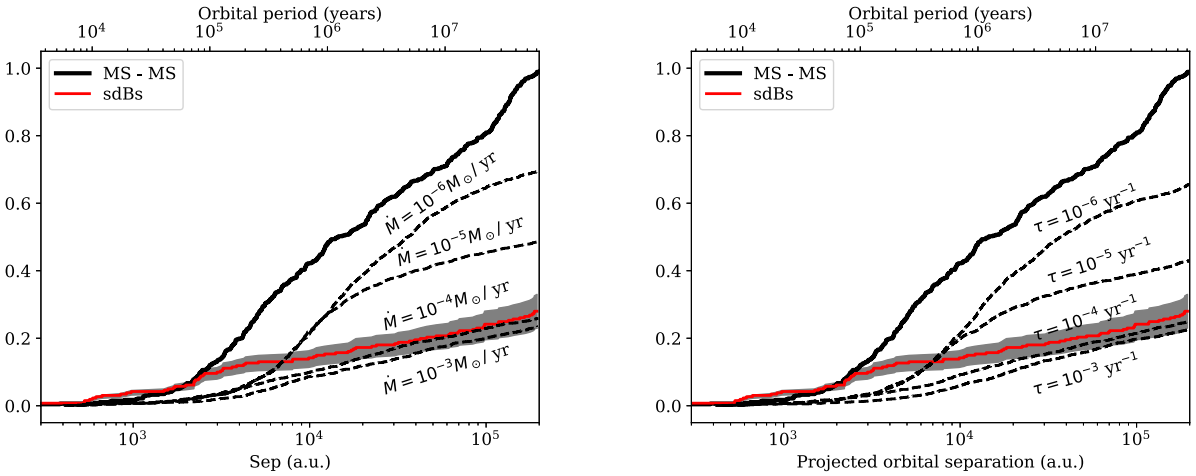

Figure 11. Results of the simulations of orbital evolution for sdBs with different mass-loss time-scales using comparison sample A as the initial sample. The final cumulative probability is multiplied by the total survival fraction. The grey area shows the 1 σ uncertainty interval. Left-hand panel – constant mass-loss rate, right-hand panel – exponentially decaying mass-loss. The final mass of the inner binary is assumed to be 0.9 $M_\odot$.

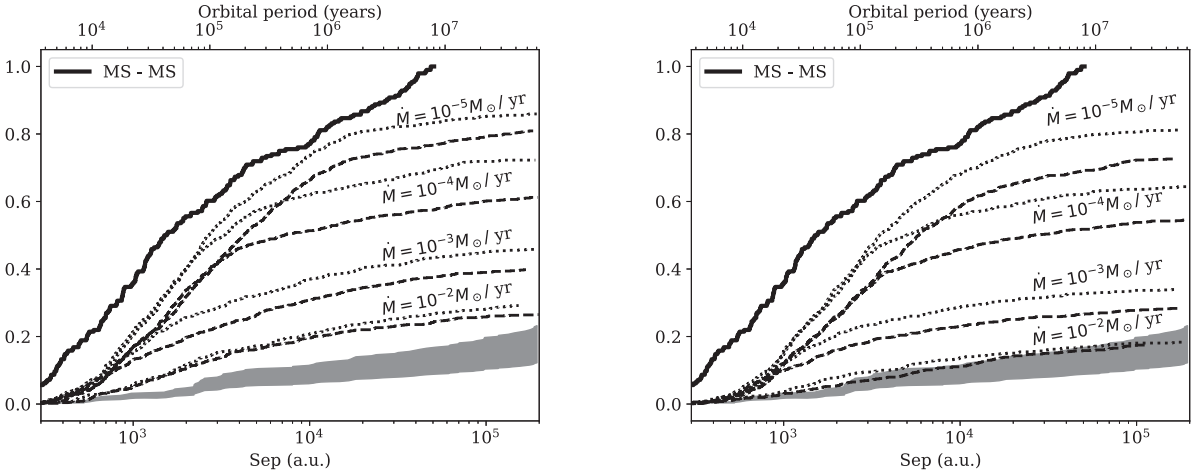

Figure 12. Results of simulations of the orbital evolution with different mass-loss time-scales for sdBs using comparison sample B as the initial sample. The left-hand and right-hand panels show simulations with the final mass of the inner binary 0.9 and 0.4 $M_\odot$ respectively. The dashed and dotted lines are for fractions excluding third components with masses less than 0.4 and 0.6 $M_\odot$, respectively. The grey area shows the uncertainty region for the survival probability of the ultrawide companions to the sdBs. The final cumulative probability is multiplied by the total survival fraction.

In this work we searched for common proper motion and parallax pairs to systems which went through a CEE using the *Gaia* DR 2. We found 68 ultrawide companions to sdBs, 6 companions to pCE and 14 companions to CVs. Future third *Gaia* data release will help us to further verify the physical association of these companions through radial velocity measurements.

We find that the ultrawide multiplicity rates for systems which went through the common envelope evolution are as follows pCE – 3.7 per cent, sdBs – 1.4 per cent and CVs – 2.5 per cent. These are 2–4 times smaller than the multiplicity rate found for the corresponding progenitor systems (ultrawide binaries to wide MSWD – 4.2 per cent, comparison samples A – 5.0 per cent, B – 7.0 per cent, C – 4.7 per cent). These differences are especially significant in the case of sdBs and CVs.

Assuming that the third companions to sdBs and CVs are bound to the central binary and share a similar physical origin, we perform simulations for the evolution of systems due to mass-loss and consider a range of possible mass-loss rates. We find that the fraction of survived ultrawide companions and the projected separations are compatible to short-term mass-loss in the case of sdB formation i.e. $\dot{M} \gtrapprox 10^{-2}\,M_\odot\,\mathrm{yr}^{-1}$. However, in the case of CVs (with the caveat of the much smaller statistics currently exiting), the results suggest much longer time-scale of a few 10^4 yr (i.e. a mass-loss rate of $\approx 10^{-4}\,M_\odot\,\mathrm{yr}^{-1}$).

Interestingly, studies of the periods of post-CE binary systems gave rise to differences in the inferred $\alpha_{\rm CE}$ parameters between lower and higher mass progenitors (Davis, Kolb & Knigge 2012). Though these issues might not be related to our study, they might possibly indicate a joint origin. Namely, it is possible that different processes govern CEE in these different systems. For example, it is possible the CEE suggested to be assisted by recombination is sufficiently efficient for low mass-stars below 3 $M_\odot$, but less effective for more massive 5–9 $M_\odot$ stars (P. Podsiadlowski, private communication). In this case the more massive progenitors of CVs would not lose their envelope through the inspiral and following phases, and might require a much longer time-scale for mass-loss through other means, e.g. through the suggested dust-driven winds mechanism (Glanz & Perets 2018) which operates on longer time-scales more consistent

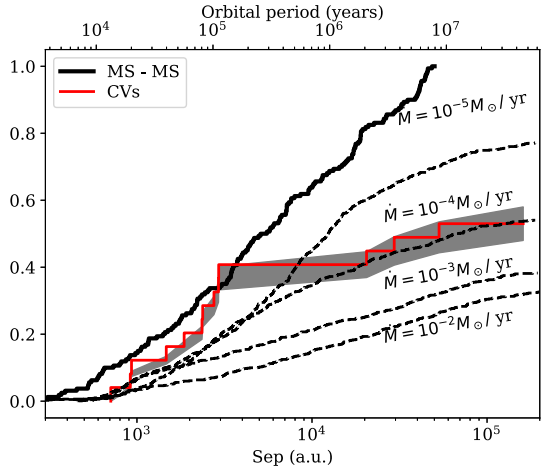

Figure 13. Results of the simulations for orbital evolution with constant mass-loss rate for ultrawide binaries with CVs. The final cumulative probability is multiplied by the total survival fraction.

with those we inferred for CVs. Such differences would significantly affect the inferred CE parameters.

Finally, CEE might be accompanied by an effective kick to the CE-system due to asymmetric mass-loss. Kicks at the level of even just a few km s^{-1} could dissociate or significantly change the distribution of third wide-companions to such systems. Such possibility would manifest itself as producing smaller fractions of wide companions and at larger separations. It is therefore possible that kicks can mimic the effects of fast mass-loss rate. In the case of sdBs for which the inferred mass-loss rate was high might be alternatively interpreted as a possible evidence for CE-kick, rather that a dynamical mass-loss in CEE. This issue, however is beyond the scope of this study and will be explored in detail elsewhere.

ACKNOWLEDGEMENTS

We would like to thank P. Podsiadlowski and M. Moe for helpful discussions. AIP thanks the Science and Technology Facilities Council (STFC) for research grant ST/S000275/1. This work has made use of data from the European Space Agency (ESA) mission *Gaia* (https://www.cosmos.esa.int/gaia), processed by the *Gaia* Data Processing and Analysis Consortium (DPAC, https://www.cosmos.esa.int/web/gaia/dpac/consortium). Funding for the DPAC has been provided by national institutions, in particular the institutions participating in the *Gaia* Multilateral Agreement.

This research has made use of the SIMBAD data base, operated at CDS, Strasbourg, France.

REFERENCES

Abt H. A., 1981, ApJS, 45, 437
Adam C., Mugrauer M., 2014, MNRAS, 444, 3459
Ambartsumian V. A., 1937, AZh, 14, 207
Andrae R. et al., 2018, A&A, 616, A8
Bailer-Jones C. A. L., 2015, PASP, 127, 994
Bailer-Jones C. A. L. et al., 2013, A&A, 559, A74
Bailer-Jones C. A. L., Rybizki J., Fouesneau M., Mantelet G., Andrae R., 2018, AJ, 156, 58
Cantat-Gaudin T. et al., 2018, A&A, 618, A93
Copperwheat C. M., Morales-Rueda L., Marsh T. R., Maxted P. F. L., Heber U., 2011, MNRAS, 415, 1381
Davis P. J., Kolb U., Knigge C., 2012, MNRAS, 419, 287
Dupuy T. J., Liu M. C., 2011, ApJ, 733, 122
El-Badry K., Rix H.-W., 2018, MNRAS, 480, 4884
Farihi J., Becklin E. E., Zuckerman B., 2005, ApJS, 161, 394
Gaia Collaboration, 2016, A&A, 595, A1
Gaia Collaboration, 2018, A&A, 616, A1
Geier S., Raddi R., Gentile Fusillo N. P., Marsh T. R., 2019, A&A, 621, A38
Gili R., Bonneau D., 2001, A&A, 378, 954
Glanz H., Perets H. B., 2018, MNRAS, 478, L12
Gontcharov G. A., 2012, Astron. Lett., 38, 694
Good S. A., Barstow M. A., Burleigh M. R., Dobbie P. D., Holberg J. B., 2005, MNRAS, 364, 1082
Götberg Y., de Mink S. E., Groh J. H., Leitherer C., Norman C., 2019, A&A, 629, A134
Green G. M. et al., 2018, MNRAS, 478, 651
Han Z., Podsiadlowski P., Maxted P. F. L., Marsh T. R., Ivanova N., 2002, MNRAS, 336, 449
Han Z., Podsiadlowski P., Maxted P. F. L., Marsh T. R., 2003, MNRAS, 341, 669
Heber U., 1986, A&A, 155, 33
Heber U., 2016, PASP, 128, 082001
Heber U., Moehler S., Napiwotzki R., Thejll P., Green E. M., 2002, A&A, 383, 938
Heggie D. C., 1975, MNRAS, 173, 729
Hills J. G., 1983, ApJ, 267, 322
Hut P., Makino J., McMillan S., 1995, ApJ, 443, L93
Igoshev A. P., Perets H. B., 2019, MNRAS, 486, 4098
Igoshev A., Verbunt F., Cator E., 2016, A&A, 591, A123
Ivanova N. et al., 2013, A&AR, 21, 59
Jordi C. et al., 2006, MNRAS, 367, 290
Jordi C. et al., 2010, A&A, 523, A48
Kepler S. O. et al., 2019, MNRAS, 486, 2169
Kupfer T. et al., 2015, A&A, 576, A44
Mace G. N. et al., 2013, ApJ, 777, 36
Mardling R. A., Aarseth S. J., 2001, MNRAS, 321, 398
McCook G. P., Sion E. M., 1999, ApJS, 121, 1
Michaely E., Perets H. B., 2019, MNRAS, 484, 4711
Moe M., Di Stefano R., 2017, ApJS, 230, 15
Mukai K., 2017, PASP, 129, 062001
Napiwotzki R., Karl C. A., Lisker T., Heber U., Christlieb N., Reimers D., Nelemans G., Homeier D., 2004, Ap&SS, 291, 321
Paczynski B., 1976, in Eggleton P., Mitton S., Whelan J., eds, Proc. IAU Symp 73, Structure and Evolution of Close Binary Systems. Kluwer, Dordrecht, p. 75
Raghavan D. et al., 2010, ApJS, 190, 1
Rebassa-Mansergas A., Gänsicke B. T., Rodríguez-Gil P., Schreiber M. R., Koester D., 2007, MNRAS, 382, 1377
Rebassa-Mansergas A., Nebot Gómez-Morán A., Schreiber M. R., Gänsicke B. T., Schwope A., Gallardo J., Koester D., 2012, MNRAS, 419, 806
Rebassa-Mansergas A., Agurto-Gangas C., Schreiber M. R., Gänsicke B. T., Koester D., 2013, MNRAS, 433, 3398
Rebassa-Mansergas A., Ren J. J., Parsons S. G., Gänsicke B. T., Schreiber M. R., García-Berro E., Liu X.-W., Koester D., 2016, MNRAS, 458, 3808
Ritter H., 2010, Mem. Soc. Astron. Italiana, 81, 849
Ritter H., Kolb U., 2003, A&A, 404, 301
Roman N. G., 1950, ApJ, 112, 554
Saffer R. A., Bergeron P., Koester D., Liebert J., 1994, ApJ, 432, 351
Saffer R. A., Livio M., Yungelson L. R., 1998, ApJ, 502, 394
Salpeter E. E., 1955, ApJ, 121, 161
Stys D. et al., 2000, PASP, 112, 354
Suleimanov V. F., Doroshenko V., Werner K., 2019, MNRAS, 482, 3622
Tokovinin A., 2014a, AJ, 147, 86
Tokovinin A., 2014b, AJ, 147, 87
Tokovinin A., Kiyaeva O., 2016, MNRAS, 456, 2070
Tuohy I. R., Buckley D. A. H., Remillard R. A., Bradt H. V., Schwartz D. A., 1986, ApJ, 311, 275
Vennes S., Kawka A., O'Toole S., Nãmeth P., Burton D., Kotze E., Buckley D. A. H., 2015, MNRAS, 450, 3514

Webbink R. F., 1984, ApJ, 277, 355
Wood K. S. et al., 1984, ApJS, 56, 507
York D. G. et al., 2000, AJ, 120, 1579
Zacharias N., Finch C. T., Girard T. M., Henden A., Bartlett J. L., Monet D. G., Zacharias M. I., 2013, AJ, 145, 44
Zenati Y., Toonen S., Perets H. B., 2019, MNRAS, 482, 1135

APPENDIX A: IDENTIFICATION OF MSWD IN THE *GAIA* DATA RELEASE

Many MSWD systems are observed as faint objects with the SDSS *g* band magnitudes in the range 16^m–22^m, while the *Gaia* is expected to be complete only until 20 mag in unfiltered light (Napiwotzki et al. 2004; Jordi et al. 2006). A significant fraction of these systems are below the photometric sensitivity of the *Gaia*. Moreover, in crowded fields the *Gaia* data base could contain up to tens of faint stars in a region with size of a few arcsec. Therefore, we decided to first identify our MSWD binaries in the *Gaia* data base based on both location and magnitude.

To practically search for counterparts, we convert the SDSS colours g,i,r to the G *Gaia* colour using the polynomial fit by Jordi et al. (2010). After this, we select all stars at angular separations less than 5 arcsec from the SDSS catalogue location and assume that the MSWD counterpart is the star which magnitude differs by less than $4\,\sigma$ from the magnitude computed according to equation from Jordi et al. (2010) and is located at the smallest angular separation from its SDSS catalogue position.

After this we manage to identify 1979 out of 3287 MSWD binaries. We plot the distribution of colour difference and parallaxes in Fig. A1. We know that in the second *Gaia* data release stars are treated as separate if the angular separation exceeds a couple of arcsec. For our typical parallax it would correspond to ≈600 au. In the real sample the shortest angular separation is ≈100 au which corresponds to an angular separation of 1.2 arcsec. There is no doubt that such systems are seen as spectral binaries in the SDSS survey. In the context of our analysis it means that a fraction of these systems are binaries and not triples.

From the list of systems we choose ones with good astrometric solution and with relative errors of parallax and proper motions smaller than 0.25. Our filtered list contains 998 NSWD binaries including 161 pCE binaries. These binaries have mean parallax 3.3 mas and mean *Gaia* G magnitude of 18.1.

APPENDIX B: ADQL REQUEST TO SELECT STARS FOR COMPARISON SAMPLES

Here we show two ADQL requests for the *Gaia* data base which helped us to form the comparison samples. The comparison sample A (larger distances) is selected as:

```
SELECT top 10000 source_id, ra, dec, phot_g_mean_mag,
parallax, parallax_error, pmra, pmra_error, pmdec,
pmdec_error, phot_bp_mean_mag, phot_rp_mean_mag,
teff_val, lum_val, radius_val
FROM gaiadr2.gaia_source
WHERE lum_val >  24
  and lum_val <  140 and teff_val > 7500
and teff_val < 10000 and radius_val > 1.4
and radius_val < 4 and parallax > 0.67
and parallax < 10
  and parallax / parallax_error > 5
and pmra / pmra_error > 5 and pmdec / pmdec_error > 5
ORDER by source_id
```

In order to select the comparison sample B (smaller distances) we use the following request:

```
select top 5000 source_id, ra, dec, phot_g_mean_mag,
parallax, parallax_error, pmra, pmra_error, pmdec,
pmdec_error, phot_bp_mean_mag, phot_rp_mean_mag,
teff_val, lum_val, radius_val, bp_rp
from gaiadr2.gaia_source
where phot_g_mean_mag
- 5.0 * log10(100.0 / parallax) < 1.2
and bp_rp < 0.35
and parallax > 5
  and parallax / parallax_error > 20
order by source_id
```

This request returns only 2452 stars.

Comparison sample C is selected using the following request:

```
select top 5000 source_id, ra, dec, phot_g_mean_mag,
parallax, parallax_error, pmra, pmra_error, pmdec,
pmdec_error, phot_bp_mean_mag, phot_rp_mean_mag,
teff_val, lum_val, radius_val, bp_rp
```

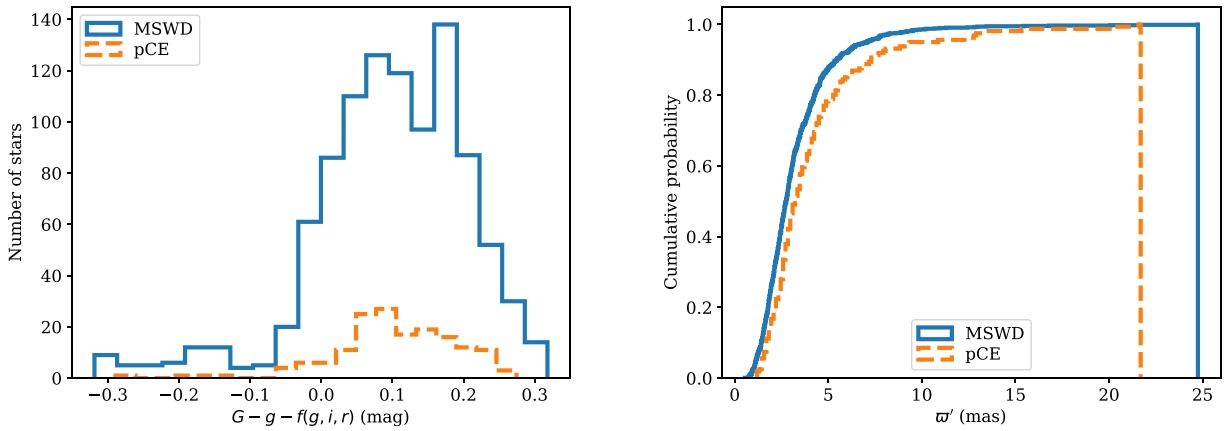

Figure A1. Left-hand panel: the histogram of the colour difference between that predicted by Jordi et al. (2010) equation and that measured for *Gaia* counterpart for general MSWD systems (solid line) and pCE systems (dashed line). Right-hand panel: the cumulative distribution of measured parallaxes for systems identified in *Gaia* DR2.

```
from gaiadr2.gaia_source
where phot_g_mean_mag
- 5.0 * log10(100.0 / parallax) < 0.0
and bp_rp < 0.35
and parallax > 2
  and parallax / parallax_error > 10
order by source_id
```

APPENDIX C: JUSTIFICATION FOR THE COMPARISON BETWEEN DIFFERENT FRACTIONS

MSWD inner binaries are wider in comparison to sdBs progenitors, which could potentially affect our conclusion. The exact reason is that the observed period distribution peaks around 50 au (Tokovinin 2014a,b) and so MSWD binaries in hierarchical triples should be more numerous than the much tigher progenitors of sdB binaries in hierarchical triples. We test this possibility using the simulation procedure described by Tokovinin (2014b). Namely, we draw 480 000 stellar systems with primary mass in the range 0.85 and 1.5 $M_\odot$ following the Salpeter initial mass function (Salpeter 1955). We classify a binary at any level of hierarchy as pre-sdB if its orbital separation is between 0.01 and 2 au and as MSWD if its orbital separation is between 10 and 200 au (systems with separations 2–10 au could go through CEE). After this classification step we count separately systems which are members of wide (tertiary at separation larger than 10^3 au) hierarchies and ones which are simply binaries. This procedure is very similar to that done in our research procedure.

As a result of this analysis, we identified 4398 pre-sdBs with tertiary companion among 66234 pre-sdBs with or without an additional companion which corresponds to roughly 6.6 per cent of all sdBs to be members of wide hierarchical systems. The same analysis for MSWD gives us 6972 MSWD are bound with ultrawide tertiary companion among 88 897 MSWD with and without tertially companion which is 7.8 per. Although 6.6 per cent differs from 7.8 per cent, the difference is only 1.2 times. Additional cuts on the ultrawide system mass ratio $Q = M2/M1 > 0.4$ slightly increases the difference up to 1.3 times. Therefore this effect cannot explain the observed difference of three times seen between ultrawide mupliplicity fraction of MSWD and sdB systems.

We compute similar values for our sample A. Namely, we classify a star as an ultrawide binary if its orbital separation is above 10^3 au. In our simulations we found 42 176 such wide binaries and 437 824 are isolated which includes 181 596 hierarchies with separations less than 10^3 au. The latter hierarchical systems are treated as isolated stars in our analysis using the *Gaia* because they cannot be resolved. These numbers correspond to 8.8 per cent of the ultrawide multiplicity fraction. This fraction is 1.3 times larger than the corresponding fraction of sdBs with ultrawide companion and it is 1.1 times larger than the fraction of MSWD with wide companion in comparison to the MSWD without any companion which is in perfect agreement with the small difference seen in Table 1. Overall, the stellar statistics could explain the difference of 1.3 times between the ultrawide multiplicity fraction for A sample and the sdB sample while the difference seen in observations is 3.6 times.

The same can be shown in a more analytical way. We restrict the discussion up to quadruples. If we use the similar notation as Tokovinin (2014b) and designate a binary with the longest orbital period (possibly with more hierarchy levels) as L1, and the inner binary around the primary as L11 and the inner binary around the secondary as L12, we can additionally introduce L11+ as triples with ultra-wide companion at separations larger than 10^3 au and L11− as triples with ultrawide companion at separations smaller than 10^3 au, so $N^{\rm L11} = N^{\rm L11+} + N^{\rm L11-}$. We can describe the number of sdBs with ultrawide companion at separations larger than 10^3 au as $N^{\rm L11+}_{\rm sdBs}+N^{\rm L12+}_{\rm sdBs}$ which is an integral of the probability density for the periods $f(P)\mathrm{d}P$ over a range of values allowing a formation of sdBs, taking into account the formation of a triple. The similar number of MSWDs with ultrawide companion is $N^{\rm L11+}_{\rm MSWD}+N^{\rm L12+}_{\rm MSWD}$. The fraction presented in Table 1 refers to the number of $N^{\rm L11+}_{\rm sdBs}+N^{\rm L12+}_{\rm sdBs}$ among all sdBs which is the sum of $N^{\rm L1}_{\rm sdBs}$ (truly isolated sdBs) and $N^{\rm L11}_{\rm sdBs}+N^{\rm L12}_{\rm sdBs}$ (resolved and non-resolved triples). So the fraction 'sdBs + distant' is:

$$f_{\rm sdBs} = \frac{N^{\rm L11+}_{\rm sdBs} + N^{\rm L12+}_{\rm sdBs}}{N^{\rm L1}_{\rm sdBs} + N^{\rm L11}_{\rm sdBs} + N^{\rm L12}_{\rm sdBs}}. \quad \text{(C1)}$$

A similar fraction of 'MSWD + distant' is:

$$f_{\rm MSWD} = \frac{N^{\rm L11+}_{\rm MSWD} + N^{\rm L12+}_{\rm MSWD}}{N^{\rm L1}_{\rm MSWD} + N^{\rm L11}_{\rm MSWD} + N^{\rm L12}_{\rm MSWD}}. \quad \text{(C2)}$$

A fraction of these equations gives:

$$\frac{f_{\rm sdBs}}{f_{\rm MSWD}} = \frac{N^{\rm L11+}_{\rm sdBs} + N^{\rm L12+}_{\rm sdBs}}{N^{\rm L11+}_{\rm MSWD} + N^{\rm L12+}_{\rm MSWD}} \frac{N^{\rm L1}_{\rm MSWD} + N^{\rm L11}_{\rm MSWD} + N^{\rm L12}_{\rm MSWD}}{N^{\rm L1}_{\rm sdBs} + N^{\rm L11}_{\rm sdBs} + N^{\rm L12}_{\rm sdBs}}. \quad \text{(C3)}$$

The first term gives ≈0.5 because MSWD are wider and cover the peak of the period distribution, but due to exactly the same reason the second term gives ≈2 so the total fraction is close to 1.

There are two fundamental reasons why we find such a small difference in statistics. First, the simulation procedure suggested by Tokovinin (2014b) assumes that the period distributions at different levels of hierarchy are independent of each other as soon as the levels are well separated (dynamical truncation factor is negligible). MSWD and sdBs well satisfy this assumption because their discoverable ultrawide companions are located at separations larger than 10^3 au. Secondly, the multiplicity fraction of binaries as compared to isolated stars and triples as compared to binaries are very similar and assumed to be 0.466 by Tokovinin (2014b).

It is interesting to note that if the multiplicity fractions at different levels of hierarchy start to differ e.g. if we interested to reproduce fraction of quadruples precisely, it affects $f_{\rm sdBs}/f_{\rm A}$ making it slightly larger 1.8 (no observational selection, taking into account sdBs around the secondary star) and $f_{\rm sdBs}/f_{\rm A} = 1.6$ (cut at $Q > 0.4$). Fraction $f_{\rm sdBs}/f_{\rm MSWD}$ stays close to 1.2. On the other hand, if we want to take into account more realistic criterion for orbital stability (Mardling & Aarseth 2001), we get $f_{\rm sdBs}/f_{\rm MSWD} \approx 0.9$ and $f_{\rm sdBs}/f_{\rm A} = 1.4$. In this case we do not reproduce the stellar statistics, because the method suggested by Tokovinin (2014b) mimics this criterion only approximately. Therefore, we expect that newer works on stellar statistics might slightly change the conclusion of our work, but we do not expect $f_{\rm sdBs}/f_{\rm MSWD}$ or $f_{\rm sdBs}/f_{\rm A}$ differ from 1 too significantly.

This paper has been typeset from a TEX/LATEX file prepared by the author.